1
2
3
4
5
6
7
8
9
10
11
12
13
14
15
16
17
18
19
20
21
22
23
24
25
26
27
28
29
30
31
32
33
34
35
36
37
38
39
40
41
42
43
44
45
46
47
48
49
50
51
52
53
54
55
56
57
58
59
60

Mechanisms of Liquid Phase Exfoliation for the Production of Graphene

Zheling Li[1,2]*, Robert J. Young[1,2,4]*, Claudia Backes[3], Wen Zhao[4,5], Xun Zhang[1], Alexander Zhukov[2,6], Evan Tillotson[1,2], Aidan P. Conlan[1,2], Feng Ding[4,5], Sarah J. Haigh[1,2], Kostya S. Novoselov[2,6,8], Jonathan N. Coleman[7]

1. Department of Materials, University of Manchester, Manchester M13 9PL, UK

2. National Graphene Institute, University of Manchester, Manchester M13 9PL, UK

3. Institute of Physical Chemistry, Heidelberg University, Im Neuenheimer Feld 253, 69120 Heidelberg, Germany

4. Institute of Textiles and Clothing, Hong Kong Polytechnic University, Hung Hom, Hong Kong

5. Center for Multidimensional Carbon Materials, Institute for Basic Science (IBS-CMCM)/School of Material Science and Engineering, Ulsan National Institute of Science and Technology (UNIST), Ulsan 44919, Korea.

6. Department of Physics and Astronomy, University of Manchester, Oxford Road, Manchester, M13 9PL, UK

7. School of Physics and CRANN & AMBER Research Centers, Trinity College Dublin, The University of Dublin, Dublin 2, Ireland

8. Chongqing 2D Materials Institute, Liangjiang New Area, Chongqing, 400714, China

Corresponding Authors

Robert J. Young (robert.young@manchester.ac.uk)

Zheling Li (zheling.li@manchester.ac.uk)

ABSTRACT

Liquid phase exfoliation (LPE) is the principal method of producing two-dimensional (2D) materials such as graphene in large quantities with a good balance between quality and cost, and is now widely adopted by both the academic and industrial sectors. The fragmentation and exfoliation mechanisms involved have usually been simply attributed to the force induced by ultrasound and the interaction with the solvent molecules. Nonetheless, little is known about how they actually occur, *i.e.* how a thick and large graphite crystals can be exfoliated into thin and small graphene flakes. Here we demonstrate that during ultrasonic LPE, the transition from graphite flakes to graphene takes place in three distinct stages. Firstly, sonication leads to the rupture of large flakes and the formation of kink band striations on the flake surfaces, primarily along zig-zag directions. Secondly, cracks form along these striations, and together with intercalation of solvent, lead to the unzipping and peeling off of thin graphite strips that in the final stage are exfoliated into graphene. The findings will be of great value in the quest to

optimize the lateral dimensions, thickness and yield of graphene and other 2D materials in large-scale LPE for various applications.

KEYWORDS: fragmentation, exfoliation, liquid phase exfoliation, 2D materials, ultrasound

    The isolation of graphene using the celebrated 'scotch tape' mechanical exfoliation method produces material of high quality for the study of fundamental physics.[1] It is, however, time-consuming with low yield, hence a number of other methods have been developed to produce graphene for large-scale applications, such as in inks, coatings, membranes and nanocomposites.[2] Among those methods, LPE, involving the exfoliation of graphite or other 2D layered materials into thinner and smaller flakes with the assistance of sonication in solvents have been found to be successful,[3-11] as it offers upscaling production and good quality at reasonable cost. Its variants, such as shear mixing,[12] ball milling[13] and microfluidization,[14] have also been developed to target certain industrial applications, which further broaden the adoption of LPE methods in industry.[15] Considerable work has been undertaken to evaluate different solvents, sonication types and sonication times, all of which are found to affect the quality of the exfoliated graphene.[5, 16-18] By having these factors tuned and optimized, a formulation and recipe can be obtained to direct the production scale-up for specific applications.[19]

    Nonetheless, despite the extensive interest from industry, the wider adoption and optimization of LPE is hindered by the lack of a fundamental understanding of the process. For example, the few-layer graphene produced is usually small with an average lateral dimensions of <1 μm and a yield only about ~20% (compared to the mass of starting bulk graphite).[20] Generally, LPE involves two simultaneous structural modifications: *exfoliation* – the reduction in thickness and *fragmentation* – the reduction in lateral dimension.[3, 13, 21-24] To a first approximation, whether or

not graphite prefers to exfoliate or fragment seems to be related to the ratio of the surface energy of the edge plane (E_E) and the basal plane (E_S) of graphite and the ratio of the out-of-plane and the in-plane mechanical properties of graphite.[21, 22] Regarding exfoliation, a good interaction of solvent with the graphene flakes is found to be necessary for the exfoliation to progress well.[24] However, the fragmentation process has been simply described as a tearing process, similar to the scission process in carbon nanotubes,[5] by sonication-induced microjets or collisions between the flakes and container (Section 1 of the Supporting Information (SI)).[13] Such descriptions are qualitative and envisage that exfoliation and fragmentation of the flakes take place simultaneously but do not reveal in detail how they take place.

It was not until recently that researchers have described fragmentation mechanisms, through statistical modelling, as a rupture process triggered by randomly-formed cracks driven by external force,[23] probably ultrasound-induced cavitation.[25, 26] A two-stage model was also suggested,[27] indicated by the bimodal distribution of flake area,[25-29] wherein large flakes rupture first followed by a possible 'erosion' process where smaller flakes are thought to emanate from the edge of the large ones,[23, 27] probably through a peeling process[29, 30] due to the hydrodynamic load.[31] Although this was speculated from statistical modelling, it is consistent with the increased surface roughness with terraces observed on the surface of exfoliated graphite.[26] In particular, such basal plane defects that lead to fragmentation were suggested to be neither vacancies nor impurities but some type of 'topological' defect.[32] It was further suggested that such chemically-active defects can be functionalized by oxygen groups.[33, 34] This plays a crucial role in promoting fragmentation as revealed by XPS on a number of 2D materials, such as hBN[35] and MoS_2,[36, 37] but details of the process are not properly understood, such as exactly where the oxygen functional groups are attached.

Given the different models covering various aspects of the LPE process, a clear understanding of the fragmentation and exfoliation process is still lacking, and the roles of the 'topological defects' and oxygen functionalization also remain unclear. This is because the existing studies have primarily focused on large-scale processing – involving thousands of flakes[23, 27] – over long periods of sonication time of up to hundreds of hours,[16] hence the mechanisms involved at different stages are difficult to separate and identify. A clearer understanding of the mechanisms is crucial as it could potentially improve the yield of LPE by, for example, eliminating the need to discard large flakes,[38] and allow optimization of the products dimensions and thickness distribution. This is important as flake dimensions are known to be vital in controlling the reinforcement of 2D fillers in composites,[39] delivering up to a 6-fold increase in thermal conductivity[40] and tuning the electrical conductivity of printed graphene films by up to three orders of magnitude.[41] In this study, we demonstrate that fragmentation and exfoliation take place during LPE in three distinct stages, with a kink-band-induced peeling process being one key step. This is revealed by using a combination of *in-situ* monitoring of the fragmentation and exfoliation of single flakes and statistical analysis of graphene flakes produced in large-scale LPE, with overall flake dimensions with 6 orders of magnitude variation and time-scales of sonication ranging from a few seconds to many hours. The extent to which this study is applicable for the exfoliation of other 2D layered materials and using a range of different solvent media is also discussed.

RESULTS AND DISCUSSION

Stage I (Flake rupture and kink band formation)

This first stage of sonication leads to the fragmentation of large graphite flakes along existing defects and the formation of small kink bands. We selected a graphite flake ~1 mm in diameter as a model for the analysis (Figure 1a). Before sonication, the flake had a rough morphology with some line features visible on the surface. After only 5 s of bath sonication in an IPA/H_2O mixture (volume = 1:1) the graphite flake ruptured into two pieces with more surface line features, not present in the raw flake, appearing after 25 s sonication (Section 2 of the SI). After 30 s of sonication, the graphite flakes ruptured into flatter pieces, with smoother surfaces that contained additional straight lines. The fragmentation and exfoliation of graphite have also been examined in other typical solvents that have usually been used in LPE process.[24] Similar morphological changes were observed in NMP and SDBS/H_2O solvents, but not in an H_2O control sample even after 65 s sonication (Section 3 of the SI). The rate of fragmentation and exfoliation in these solvents are in good agreement with the LPE process with large-quantity flakes.[18]
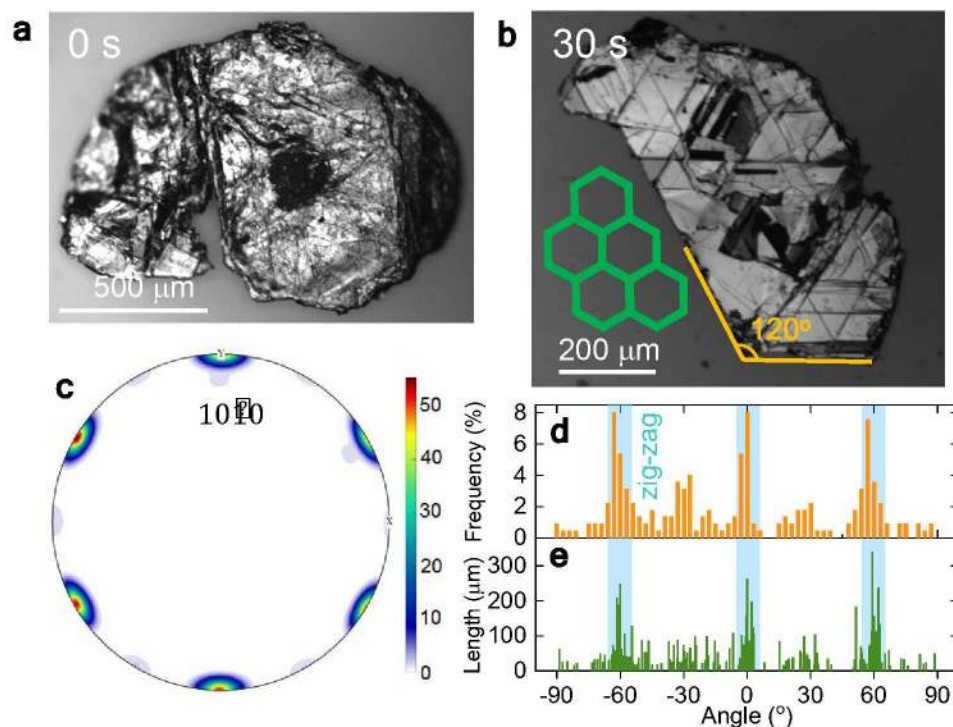
Figure 1. Structural analysis of kink bands and twins in LPE graphite. (a) Optical micrograph of a graphite crystal. (b) Optical micrograph of a large fragment of the same crystal following sonication for 30s. The inset is the crystallographic orientation of the graphite lattice determined by (c) $\{10\bar{1}0\}$ pole figure in electron backscatter diffraction (EBSD). (d) Frequency and (e) length distribution of the kink bands visible in (b) (the reference 0° direction is set as the zig-zag (ZZ) direction).

Figure 1b shows a large fragment obtained after 30s sonication in IPA/H$_2$O. Its crystallographic orientation, determined using EBSD (Figure 1c), is shown schematically as an inset. The graphite flake has a smooth surface with its long edges and lines on the surface predominantly parallel to the ZZ directions (Figure 1d). Less common, but also visible, are line features parallel to armchair (AC) directions. This implies that the line features on the surface of the flake are related to the kink bands, containing twin boundaries, reported by Rooney *et al.*[42]

(Section 4 of the SI). The kink bands follow ZZ or AC crystallographic directions and involve slip in the perpendicular directions. Particularly noticeable is that the line features observable in ZZ direction are much longer and wider than those along AC directions (Figure 1e).
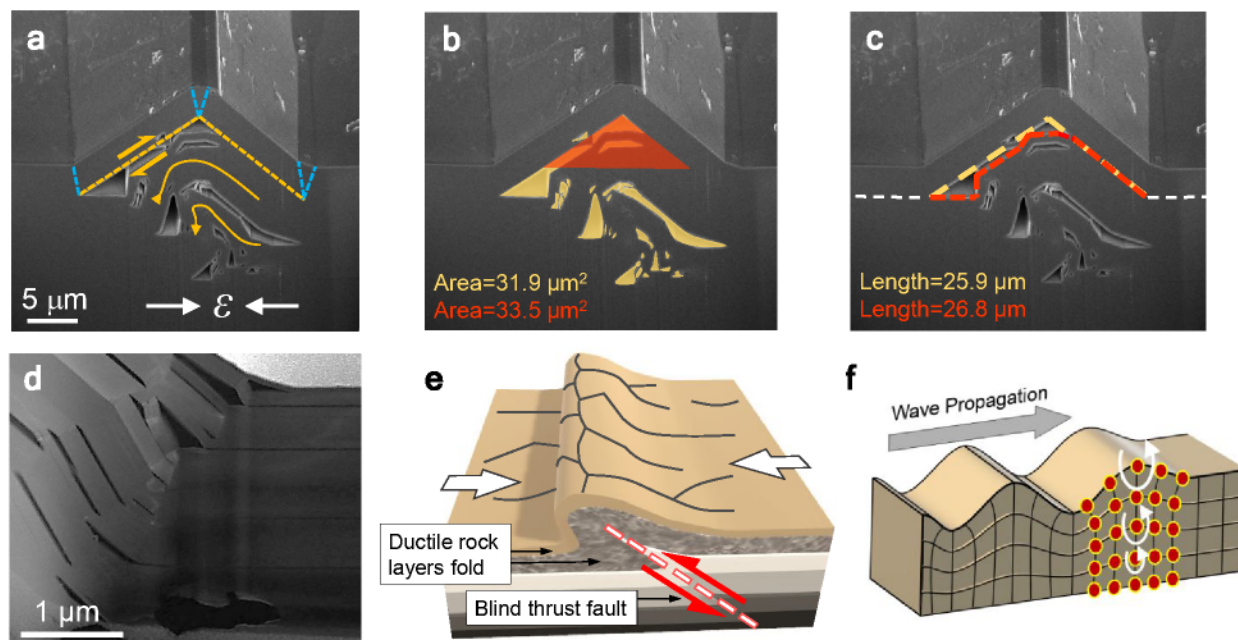

Figure 2. Analysis of Cross Sections of Kink Band Striations. (a) SEM micrograph of a sub-surface FIB-milled cross section for one kink band striation lying along the ZZ direction. The twin boundaries in the layer are shown by dotted blue lines. The direction of shear along the main fault and the expected directions of flow of the material under the surface are indicated by orange arrows. The direction of in-plane compression is indicated by the horizontal arrows. (b) Area of the voids (highlighted in yellow) and area of material protruding from the surface (highlighted in red). (c) Lengths of the top layer (yellow dashed line) and material sheared underneath (red dashed line). (d) Annular dark field (ADF) STEM image showing delamination within the kink band. Note the dark vertical bands are due to uneven thinning (curtaining) resulting from the presence of voids in the lamella cross section. (e) Schematic diagram of a blind thrust fault in a stratified rock formation.[43] The shear of the layers and the in-plane

compression direction are indicated by red and white arrows, respectively. (f) Schematic diagram

of a Rayleigh wave showing the motion of particles (red dots, also represented by the grid) close

to the surface of a material and the motion of the wave.[44]

A focused ion beam (FIB) milled cross section through a kink band striation along the ZZ

direction is shown in Figure 2a and Section 5 of the SI. It has undergone local twinning to form

hinges that allowed it to deform without fracturing. A complex pattern of damage and voiding

below the surface is observed resulting in a triangular section of the crystal pushed up from the

surface. The area of the voids and the triangular section is equivalent, suggesting that any

increase in volume produced by the voiding is compensated for by the triangular region (Figure

2b). The main damage is a shear of the top ~3 μm layer of the crystal over the material

underneath as indicated by the arrows (Figure 2a), characterized by the similar lengths of both

sides of the interfacial regions in the sheared region (Figure 2c). The overall deformation process

is illustrated in Figure 2a where the pattern of flow underneath the surface is shown to occur

through a combination of basal plane slip[45] and twinning.[42] Local delamination within the twin

boundaries is also visible (Figure 2d and Section 5 of the SI).[42] The damaged structural (Figure

2a) bears a similarity to features known as "blind thrust faults" seen in geological strata (Figure

2e),[43] found near tectonic plate margins, that occur as the result of plate margin collisions. Their

role in the initiation of earthquakes is discussed in Section 6 of the SI.

The damage of the graphite flakes can be attributed to the ultrasound, where waves are

produced from the collapse of bubbles during cavitation[13, 46] that cause a localized increase of in-

plane compression[33] and temperature.[46] The waves are transferred from the solvent to the liquid-

solid interface through Scholte waves that may then be converted into surface acoustic waves

(SAWs, *e.g.* Rayleigh waves) in the graphite.[44] Rayleigh waves propagating across the surface of

the graphite will induce an elliptical vibration of carbon atoms consisting of longitude and vertical vibration components that lead to the curved movement of material, and their amplitude decreases exponentially with depth (Figure 2f and Sections S7 and S8 of the SI).[44] Consequently, when a SAW is propagating across graphite flake, kink bands may nucleate around existing defects or where waves collide,[26] alternatively it could also cause the graphite layers to slide over each other (Figure S9). It has also been reported recently that kink bands in 2D materials can also be formed by laser shock[47] (also known to produce SAWs[44]) or fast cooling.[48]

Stage II (Peeling off of thin graphite strips)

We also examined sonicated graphite flakes in more detail to characterize the specific damage induced. A flake containing ZZ kink band traces intersecting each other at 60° with a split along one of the traces, indicated by the red arrows, is shown in Figures 3a&b. Figures 3c&d show that the exposed edges are rich in oxygen and depleted in carbon, implying that the sonication process leads to a change in the surface chemistry of the graphite flake.[49]
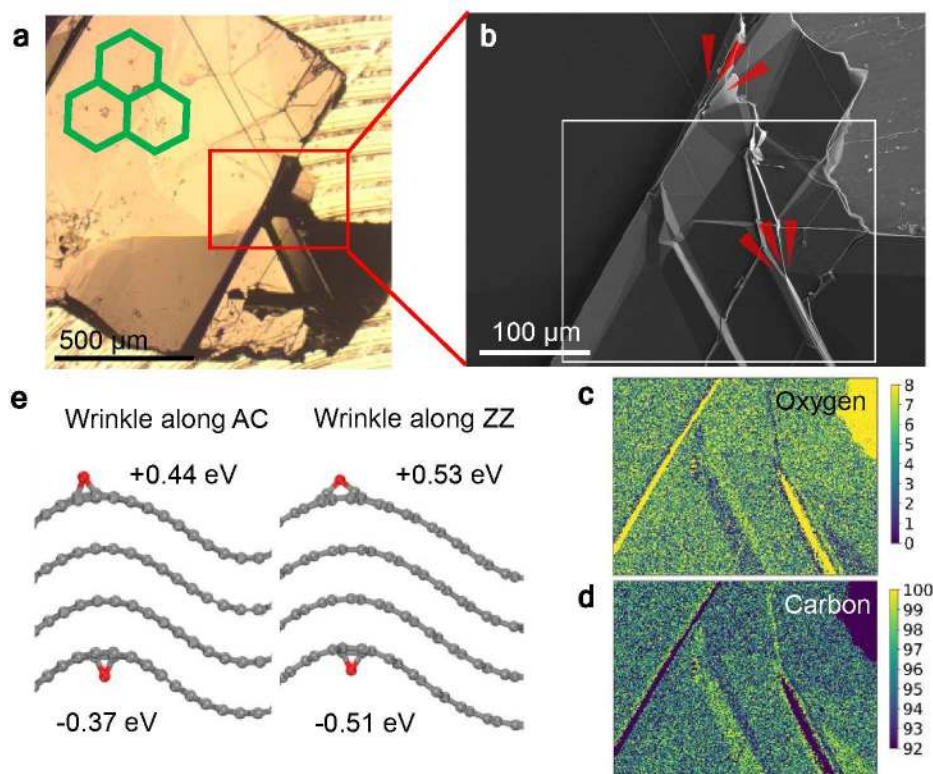
Figure 3. Cracking and modification of the surface chemistry of the kink bands in LPE graphite. (a) Optical micrograph of a graphite flake damaged through sonication for 12 s in IPA/H$_2$O (vol=1:1) using a tip sonicator. The lattice orientation determined using EBSD is shown by the green hexagons. (b) SEM micrograph of the kink band region highlighted by the red box in (a) showing the intersection of kink band traces and unzipping as indicated by red arrows. SEM EDX elemental mapping of (c) oxygen and (d) carbon in the area within the white box shown in (b) Color scale is in wt%. (e) DFT calculations of the absorption energies for oxygen atoms on bending defects along the AC and ZZ directions in graphite. For graphene planes folded along AC directions, the absorption energies of oxygen atoms outside and inside the wrinkle are 0.44 eV higher and 0.37 eV lower than that of the flat graphene, respectively. For graphene planes bending along ZZ directions, the absorption energies of oxygen atoms outside and inside the wrinkle are 0.53 eV higher and 0.51 eV lower than that on the flat graphene, respectively.

The DFT simulation shows that the high curvature where the kink bands reach the surface leads to an increase in chemical activity (Figure 3e).[42] Curved planes along ZZ directions are found to be slightly more active than those along the AC direction with the same level of in-plane compression.[34, 50, 51] Consequently, the higher chemical activity along the ridges of ZZ kink bands, along with the greater likelihood of ZZ kink bands inducing local stacking faults,[42] results in the cracks propagating predominantly along ZZ directions (Figure 3b). This is analogous to the longitudinal unzipping of carbon nanotubes[52] and strain-induced rupturing of graphene by oxidation,[51-53] both of which also occur mainly along the ZZ direction. These findings explicitly reveal the exact location of oxygen on the exfoliated flakes which play a crucial role in fragmenting flakes that could not be identified in earlier investigations upon graphene[33, 34] and other 2D materials.[35-37] It is worth noting that the oxygen species are chemically bonded to graphene/graphite as a result of the higher chemical activity of the ridge of kink bands (Figure 3e), which is confirmed by their presence even after the removal of absorbants and impurities (Section 9 of the SI).[34] It suggests that although the fragmentation of graphite is a physical/mechanical process,[28] it also involves sonochemical processes.[49, 50]

The structural changes during the fragmentation and exfoliation can also be captured using Raman spectroscopy.[42] The Raman spectra of the intact graphite and graphite with ZZ kink bands differ (Section 10 of the SI). Specifically following sonication, the intensities of the 2D1 component of the 2D band[42] and D band increase significantly over the kink band, suggesting the presence of stacking faults and exposed graphene edges.[33] This structural change demonstrates that the presence of oxygen on the ridges is indeed from oxidation of defective regions rather than, for example, residual water. Further Raman analysis of the crystal in Figure 1b shows

considerable damage through the generation of stacking faults, local strain, unzipping and micro-

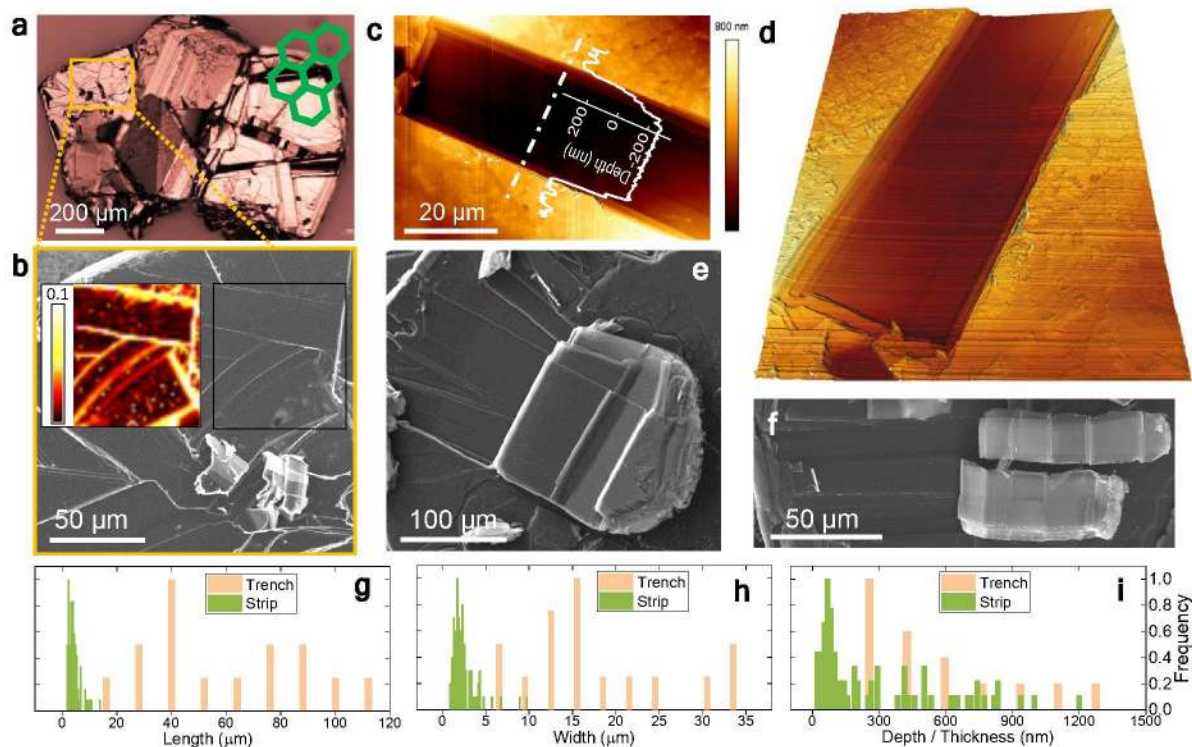cracking (Section 10 of the SI).

Figure 4. Graphite strips peeling off the parent flakes. (a) Optical micrograph of a graphite

flake sonicated in an IPA/H_2O mixture for 40 s. (b) SEM micrograph of the region in the top left

corner highlighted in yellow showing trenches and strips of material peeled from the surface of

the flake (Inset - Raman map of the area outlined in black showing an increased I_D/I_G at the

edges of the trenches). (c) AFM micrograph of a trench and the depth scan along the broken line

showing that the trench is around 400 nm deep and has stepped edges. (d) 3D view of the AFM

micrograph in (c). (e, f) Strips of multi-layer graphene material peeled back from the edges of the

flake, containing transverse AC kind band striations, and with stepped edges similar to the

trenches. (g-i) Distributions (normalized frequency) of the lengths, widths and depth or thickness

of different trenches and peeled strips determined using AFM.

We also examined a number of other sonicated graphite crystals and a typical one, subjected to ultrasound for ~40 s, is shown in Figure 4a. The surface has a number of features where material has peeled away, perhaps due to the fluid force,[31] leaving trenches (Figure 4b). The inset in Figure 4b shows an increased intensity ratio of the Raman D and G bands (I_D/I_G) at the edges of the trenches, indicating the presence of graphene edges after the unzipping and peeling of the graphite layers. The trench has a depth of around 400 nm and its edges contain steps (Figures 4c&d), that are seen to occur widely in sonicated graphite crystals along with the exfoliation of graphite strips (Figures 4e&f). The strips peeled back from the surface of the crystals also contain kink bands that are at 90° to the edges of the strips implying that they are mainly parallel to the AC direction, as the edges of the strips are generally along the original ZZ kink band striations. The strips are usually peeled off at the edges of parent graphite flakes, and eventually exfoliated further to few-layer graphene, as will be discussed later (Figure 5 and Section 10 of the SI).[31] The separation of peeled small graphite fragments from the larger parent flakes explains the previously reported bimodal distribution of the lateral sizes for exfoliated flakes.[25-28]

It is of interest to determine the lengths (*L*), widths (*W*) and depth/thickness of both the trenches and the material peeled from the parent flakes for Stage II (Figures 4g-i). Although there are wide distributions it can still be seen that the trenches and strips have comparable depth/thickness whereas the lateral dimensions of the strips are an order of magnitude less than the trench dimensions. This is clear evidence that in Stage II fragmentation is more likely to occur through the peeled strips undergoing further fragmentation along kink bands that form during the peeling process (Figures 4e&f), with much less exfoliation occurring. A similar phenomenon has been observed for other popular solvents of large-scale LPE, such as NMP and

SDBS/H$_2$O.[24] They are both found to assist the exfoliation process, and the peeling of graphite

strips occurs only within seconds of sonication (Section 3 of the SI).

Stage III (Exfoliation to thin flakes)

In order to investigate how the fragmentation and exfoliation mechanisms influence the mass

production of 2D flakes using LPE, we exfoliated a large quantity of graphite, and their lateral

dimensions ($\sqrt{LW}$), where L is the flake length and W is its thickness, and thicknesses (number

of layers, N) measured at different stages of sonication are shown in Figure 5a. In bulk scale

LPE, the more commonly-used graphite flakes with smaller dimensions were used as received

for a resolvable flake size and also to benchmark with existing studies. This is different from the

single-flake experiments described above, where only large flakes were selected from the raw

flakes in order to resolve, in detail, features that were produced in the LPE process, *e.g.* kink

bands, and also to minimize the possible damage in handling when analyzing smaller flakes. The

data points all follow approximately the same trend over many orders of magnitude regardless of

the solvent, sonication method and time, confirming that the degree of fragmentation and

exfoliation processes is governed by the intrinsic properties of the graphite,[21] while the choice of

solvent mainly affects their exfoliation rate (Sections 3 and 11 of the SI). In the LPE process,

energy in the form of ultrasound is consumed for both fragmentation (to generate new edges) and

exfoliation (to generate new surfaces) of graphite. The dimensions and thickness of the thin

graphene in Stage III are determined by the ratio of the surface energies of the edge planes (E_E)

and the basal planes (E_S) through:[21]

$$\sqrt{LW}/Nt = 2aE_E/E_S \tag{1}$$

where a is a constant, ideally equal to 1, and t is the thickness of monolayer graphene ~0.34

nm.[21] For the Stage III (Figure 5a), the dark red line, plotted using the value of $E_E/E_{S(\text{Stage III})}$=54

as reported earlier for graphene,[54, 55] matches the experimental data well when $N < \sim 30$, above which a small deviation is seen (to be discussed later).
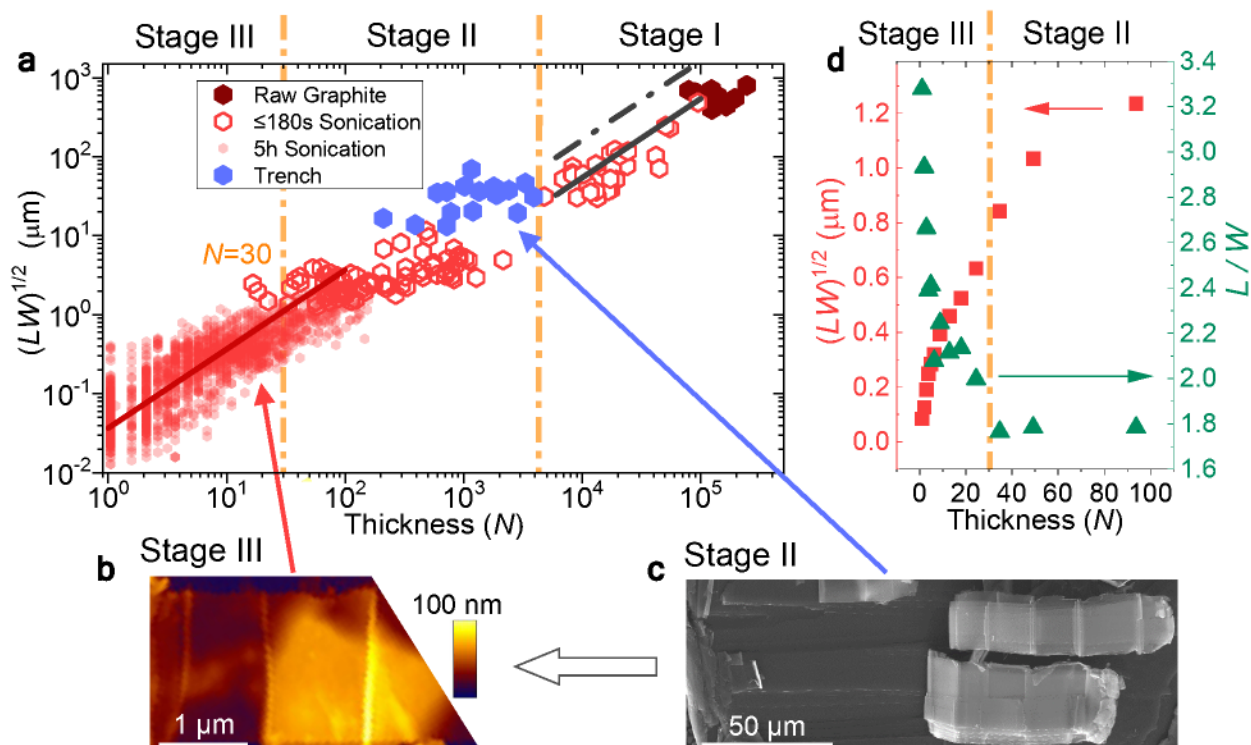

Figure 5. Different stages of the fragmentation and exfoliation processes, as separated by the broken orange lines. (a) Variation of $\sqrt{LW}$ with N of graphite/graphene in LPE, determined using a combination of interferometry (for large/thick flakes) and AFM (for small/thin flakes) (Section 14 of the SI). The material in Stage III was produced by tip sonication for 5 h in aqueous in sodium cholate and subsequent centrifugation whereas the other materials were produced by bath sonication in IPA/H₂O for periods up to ~ 180 s without centrifugation (Section 11 of the SI). The solid black and dark red lines are drawn with a slope of unity, using equation 1, with $E_E/E_{S(\text{Stage I})} = 8$ and $E_E/E_{S(\text{Stage III})} = 54$, respectively. (b) AFM image of an exfoliated graphene flake showing kink bands. (c) SEM micrograph of graphite strips with kink bands that had peeled but still remained on the parent flake. (d) Averaged $\sqrt{LW}$ and L/W of exfoliated graphene as function of N (Section 13 of the SI).

Overall Process

We have found that equation 1 can also be used to describe Stage I. The solid black line (Figure 5a) drawn for Stage I fits the experimental data very well, with $E_E/E_{S(Stage I)}$=8. However, this $E_E/E_{S(Stage I)}$ value is lower than that determined experimentally for graphite ~24 (broken black line).[55-57] The discrepancy is probably the result of processes occurring during LPE that lead to a reduction in E_E for graphite, such as oxidative attack, or an increase in E_S due to the separation of the graphene layers being reversible at the edges. The data in Stage II are, however, quite different from those in Stages I and III. This because the processes are not described by equation 1, as kink band formation and the peeling of graphite strips in Stage II affect the balance of energy consumption between fragmentation and exfoliation. The trenches (blue dots in Figure 5a) have a larger $\sqrt{LW}$ but a similar thickness N to the graphite strips collected during Stage II (red points in Stage II), as a result of the fragmentation of the peeled strips (Figures 4e-i). Although the kink bands are only associated with the early stages of LPE, until N~30, they lead to graphite strips being peeled off the parent flake. After being peeled off, the peeled strips undergo further fragmentation and exfoliation in Stage III and eventually become exfoliated graphene flakes, as evidenced by the structural similarities between graphite stripes that have been peeled off the parent flake and exfoliated kinked/twined graphene flakes (Figures 5b and c). The geometry of the peeled graphite strips, determined by the density of kink bands, will strongly affect the geometry of the exfoliated graphene (Section 12 in the SI). It is found that for a starting graphite with a higher defect density, both the lateral dimension and thickness of the exfoliated flakes drop much more rapidly in the LPE process than for an original graphite with a lower defect density (Section 12 of the SI).[29]

The data from Figure 5a in Stage III and the transition to Stage II are averaged and replotted on linear scales in Figure 5d, along with the dependence of L/W on N, in order to investigate the deviation of the experimental data from equation 1 when $N>\sim30$. A transition occurs at $N\sim30$, where $\sqrt{LW}$ starts to decrease more rapidly, due to the fact that the likelihood of kink band formation starts to diminish and bending of flake becomes preferred.[42] This is also reflected by an increase of L/W at $N\sim30$, from the average $L/W<2$ for thicker graphene to $L/W\sim3.4$ as N decreases (Figure 5d and Section 13 of the SI), in agreement with value $L/W\sim2.5\text{-}3.0$ demonstrated before.[16, 23] When the chance of kinking/twinning decreases at $N<30$, secondary mechanisms, *e.g.* tearing from edges which is more likely to produce longer strips of graphene,[32] starts to dominate the fragmentation process.[58] Any further exfoliation will take place primarily through interlayer sliding or intercalation, as envisaged in earlier studies (Section 13 of the SI).[5, 59]
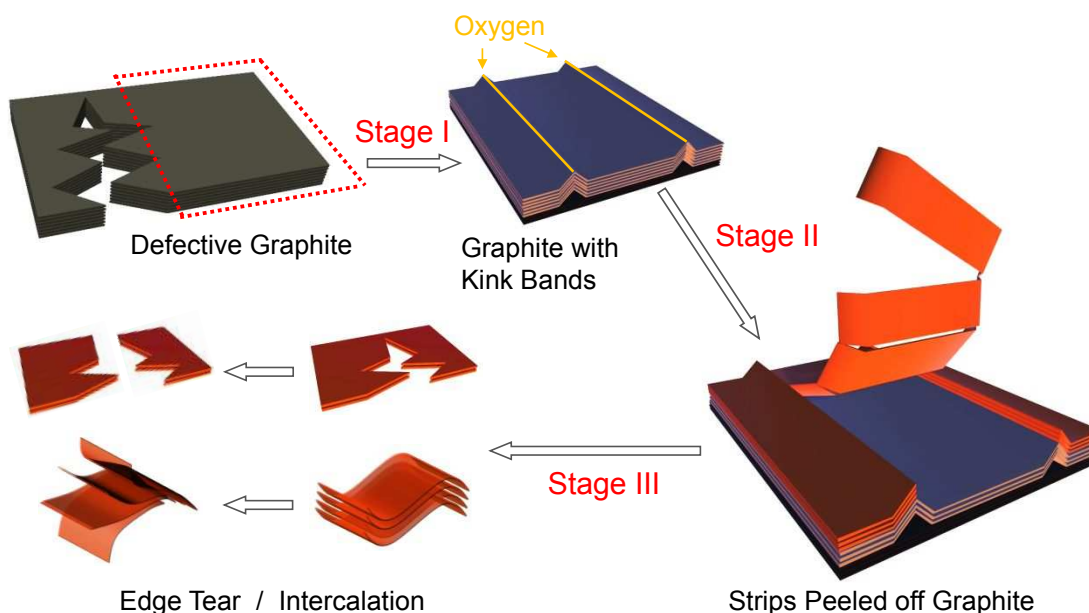

Figure 6. Three stages of fragmentation and exfoliation during LPE. Stage I (flake rupture and kink band formation): large graphite flakes break into smaller ones through existing defects

in the flakes, while the formation of kink bands also occurs. Stage II (peeling off of thin graphite strips): rupture of graphene at the ridges of kink bands and unzipping through attack by oxygen species during cavitation. This leads to the peeling off of graphite strips in which further kinking and fragmentation also take place. Stage III (exfoliation to thin flakes): the peeled graphite strips undergo further fragmentation and exfoliation until their thickness drops below $N{\sim}30$ where other fragmentation mechanisms, *e.g.* tearing, possibly start to dominate.

Consequently, the fragmentation and exfoliation process can be summarized as the following three stages (Figure 6):

Stage I - Flake rupture and kink band formation. SAWs generated from ultrasound appear to cause a complex amount of damage that includes crystal fragmentation and kink band formation. The kink band striations on the crystal surface generally lie along the ZZ direction and mask a considerable amount of sub-surface damage. At this stage, fragmentation primarily follows the existing large defects or those newly generated that penetrate through the whole thickness of the flakes (Figure S1).

Stage II - Peeling of thin graphite strips. The wavelength of the SAW running across the graphite crystal determines the penetration depth of kink bands/twins. The majority of the twins in large crystals appear to penetrate only the flake surface (Figure 2 and Section 5 of the SI). They have highly-strained and chemically-active ridges that can undergo oxidative attack due to chemical species produced by cavitation in the solvents. Their fracture results in the graphite strips between kink bands/twins being 'peeled off' from the surface of the graphite flake. The peeled graphite strips are eventually exfoliated to produce the thin graphene flakes that are usually collected as the final product of LPE.[32] The lateral dimension and thickness of the strips that are peeled off, or the exfoliated graphene, depend on the density and penetration depth of the

kink bands, while the lateral dimensions and thickness of the parent flake reduce only slowly. This separation of small graphite fragments from the large parent flakes explains the bimodal distribution of graphene observed previously.[25, 27] As the sonication time increases, more of the larger parent flakes will become fragmented and hence the lateral size distribution narrows.[28] This mechanism could also explain the phenomena that were observed previously during the LPE of BN[35] and MoS$_2$.[36, 37] The rate of the peeling-off depends on the interaction between graphite and the solvent.[35]

Stage III - Exfoliation to thin flakes. The fragmentation and exfoliation mechanism through a combination of basal plane slip and kink band formation with associated twin boundary formation discussed above only applies to thick graphite, *i.e.* the early stage of LPE. The peeled graphite strips are further exfoliated into thin graphene (Figure 5b and c). However, the kinking and peeling processes diminish when the number of graphene layers approaches ~30, as demonstrated by our previous study. This showed that for thin graphite flakes there is energetically a competition between bending and kinking/twinning and that flake below ~30 layers thick will be unlikely to undergo kinking/twinning and subsequent peeling.[42] This is consistent with the observation that after this stage any further reduction of the number of layers and lateral dimension of graphite flakes becomes much more difficult even with significantly longer sonication times.[5] This is thought to be the reason why it is difficult practically to efficiently obtain graphene flakes with large lateral dimensions and small thickness,[12] and why the yield of monolayer graphene in LPE is not particularly high.[16]

Although the present study has dealt only with LPE using ultrasound it is possible that similar damage will be induced during other types of LPE, such as high shear mixing,[12] as the result of shockwaves caused by the collision events in the container (Section 15 of the SI). It is also

shown in Section 16 in the SI that other 2D layered materials undergo similar processes. This is because the analogous mechanisms of kinking, twinning and basal-plane slip are known to occur in hBN and transition metal dichalcogenides,[42] as are their oxygen-assisted fragmentation and exfoliation.[35-37]

These findings can be used to direct the mass production of graphene using LPE. For example, the parent flakes produced in Stage II are large and thick so usually discarded in a cascade process.[16] Hence an increased production of the 'graphite strips', *e.g.* through increasing the density/penetration depth of kink bands, could be key to improving the yield of few-layer graphene and other 2D materials produced by LPE. In addition, optimization of the density/penetration depth of kink bands could also lead to a larger $\sqrt{LW}$ and smaller N for the exfoliated graphene. This might be realized by adjusting the sonication conditions such as increasing power or time.[16]

CONCLUSIONS

In summary, three stages occurring during LPE of graphite using ultrasound have been identified, each with different mechanisms involved. In Stage I, ultrasound first causes the rupture of entire flakes following large existing defects, and causes a complex amount of damage as the result of basal plane slip and the formation of kink bands containing twin boundaries. In Stage II, the highly-strained and chemically-active kink band striations undergo oxidative attack from species produced by cavitation in the solvents. The ridges of the kink bands fracture by unzipping that results in strips of thin graphite between the kink bands being 'peeled off' from the surface. These then undergo further fragmentation and exfoliation in Stage III to produce few-layer graphene flakes. These findings offer the rationale to optimize the yield, lateral

dimensions and thickness of graphene and other 2D materials produced by LPE through controlling the density/penetration depth of kink bands or/and the sonication conditions. Its applications can be anticipated to extend to other 2D layered materials and other types of LPE, such as high shear mixing, which will find even wider industrial applications.

METHODS

Liquid Phase Exfoliation. The single flake exfoliation process was studied using selected large graphite flakes (Branwell natural graphite, grade 2369) mixed with different solvents, such as an IPA/H_2O (volume=1:1) mixture, sodium dodecylbenzenesulfonate (SDBS)/H_2O (7 mg/ml) mixture and deionized H_2O.[18, 60] The vessel with a single graphite flake was either sonicated in a sonication bath (37 kHz, ~820W, Elmasonic P70H, Elma Schmidbauer GmbH), or mounted onto a metal stub and sonicated using a sonication tip (13 mm in diameter) coupled with a sonic dismembrator (20 kHz, ~700W FB705, Fisher Scientific). Flake fragments were removed during the sonication process and examined at different stages of sonication (mostly less than 100 s). The distribution of lateral dimension and thickness of bulk quantities of graphite (Stages I and II) was studied using graphite flakes (332461, Sigma-Aldrich) sonicated in an IPA/H_2O (1:1) mixture in the same sonication bath for a short time. In addition, exfoliated graphite/graphene subjected to 5h sonication (Stage II and III) was obtained as previously reported.[21] In brief, Sigma Aldrich graphite (332461) was probe sonicated (Sonics VXC-500, *i.e.* 500 W, probe diameter 13 mm) in an aqueous sodium cholate (SC) solution for 5 h. To facilitate AFM analysis, which is challenging on polydisperse samples, the as-obtained dispersion was subjected to size selection by liquid cascade centrifugation as detailed elsewhere.[21] Centrifugation was performed at 100 *g*, 400 *g*, 1 k*g*, 5 k*g*, 10 k*g*, 30 k*g*. All sediments were analyzed by statistical AFM. To obtain nanosheets with intermediate thicknesses and lateral dimensions (*i.e.* between Stage II and

III), the as-sonicated dispersion was centrifuged at 30 g, and the sediment collected. This sample was left to settle overnight to allow non-exfoliated material to sediment and the supernatant analyzed. Exfoliated graphite/graphene prepared using IPA/H_2O with a 0.5 h sonication time was obtained by sonicating with graphite powder (Sigma Aldrich graphite-332461) in a bath-sonicater (Branson CPX3800) and centrifuged for 2 h at 30 g to remove unexfoliated crystallites as sediment. The supernatant was decanted and drop-cast on Si/SiO_2 for AFM analysis.

Characterization. The materials were characterized using a range of techniques such as optical microscopy (Eclipse LV100ND, Nikon), atomic force microscopy (QI^{TM} mode, NanoWizard 4, JPK Instruments) and white light interferometer (Contour GT, Bruker). Raman spectroscopy (inVia Raman spectrometer, Renishaw) was conducted using laser λ=633 nm and a grating of 1800 line/mm. The laser power was kept low to avoid damage (<1 mW). For Stage III graphite, AFM was carried out on a Dimension ICON3 scanning probe microscope (Bruker AXS S.A.S.) in ScanAsyst in air under ambient conditions using aluminum-coated silicon cantilevers (OLTESPA-R3). Corrections established earlier were applied to thickness[12] and length,[61] respectively (Section 14 of the SI).

Scanning Electron Microscopy (SEM)/Energy-dispersive X-ray spectroscopy (EDX)/Electron Backscatter Diffraction (EBSD) were carried out using a Sigma VP FEG-SEM (Zeiss). The samples were removed during LPE process and mounted onto an SEM stub for analysis. For EBSD analysis, the sample was mounted on a 70° pre-tilt sample holder, and an accelerating voltage of 20 kV with a step size of 0.7 μm in x and y directions. EBSD patterns were collected and indexed with Aztec software. The MATLAB MTEX 5.2.3 toolbox is used for plotting the orientation data.

Focused ion beam (FIB) milling was carried out using a hybrid FIB-SEM system (Carl Zeiss Crossbeam 540). For most cases a 30 kV Ga ion beam was employed. On two occasions the final cross-section polishing has been completed using 5&2 kV beams. Final polishing was made with beam currents of up to 2 pA. The SEM images were obtained using an in-lens and secondary electron detector with compensation for 54° tilt.

Density functional theory (DFT) calculations were performed with the Vienna *ab initio* Simulation Package (VASP).[62] The exchange-correlation functional was described by the Perdew-Burke-Ernzerhof version of the generalized gradient approximation[63] and the core region by the projector augmented wave method[64] with the cutoff of plane wave set as 400 eV. The van der Waals (VDW) interaction is described by the Tkatchenko-Scheffler method.[65] A $1\times1\times1$ k-point mesh is used for absorption of oxygen atoms on the ridge, which is formed by compressing a flat graphene layer by 10%. The vacuum layer was larger than 0.8 nm to avoid interactions of neighboring images. All structures were fully relaxed until the force on each atom was less than 10^{-5} eV/nm, using the plane-wave-based total energy minimization.

AUTHOR INFORMATION

Corresponding Authors

Robert J. Young (robert.young@manchester.ac.uk)

Zheling Li (zheling.li@manchester.ac.uk)

Author Contributions

Z.L. and R.J.Y. conceived the project; Z.L. performed exfoliation of single flake and bulk flakes with short sonication time and the associated characterizations; C.B. and J.N.C. carried out

exfoliation of bulk flakes with long sonication time and the associated characterizations; A.Z. carried out FIB preparation. A.Z., E.T. and A.P.C. carried out TEM characterization. X.Z. and Z.L. performed EBSD characterization and analysis. W.Z. and F.D. performed DFT calculations; The manuscript was written through contributions of all authors. All authors have given approval to the final version of the manuscript.

ASSOCIATED CONTENT

Supporting Information Available: Fragmentation of Large Graphite Crystals by Ultrasound; Exfoliation in in Different Liquid Phases; Kinking/Twinning in Graphite; Analysis of Cross Sections of Kink Band Striations; Blind Thrust Faults and Earthquakes; Twinning in Metals Induced by Ultrasound; Seismic Waves, Earthquakes, SAWs and Exfoliation; Detailed Analysis of a Graphite Fragment; Detailed Analysis of the Relation between $\sqrt{LW}$ and N. This material is available free of charge *via* the Internet at http://pubs.acs.org.

REFERENCES

1.   Novoselov, K. S.; Geim, A. K.; Morozov, S. V.; Jiang, D.; Zhang, Y.; Dubonos, S. V.; Grigorieva, I. V.; Firsov, A. A. Electric Field Effect in Atomically Thin Carbon Films. *Science* **2004,** 306, 666-669.

2.   Novoselov, K. S.; Falko, V. I.; Colombo, L.; Gellert, P. R.; Schwab, M. G.; Kim, K. A Roadmap for Graphene. *Nature* **2012,** 490, 192-200.

3.   Coleman, J. N.; Lotya, M.; O'Neill, A.; Bergin, S. D.; King, P. J.; Khan, U.; Young, K.; Gaucher, A.; De, S.; Smith, R. J.; Shvets, I. V.; Arora, S. K.; Stanton, G.; Kim, H.-Y.; Lee, K.; Kim, G. T.; Duesberg, G. S.; Hallam, T.; Boland, J. J.; Wang, J. J. *et al.* Two-Dimensional Nanosheets Produced by Liquid Exfoliation of Layered Materials. *Science* **2011,** 331, 568.

4.   Blake, P.; Brimicombe, P. D.; Nair, R. R.; Booth, T. J.; Jiang, D.; Schedin, F.; Ponomarenko, L. A.; Morozov, S. V.; Gleeson, H. F.; Hill, E. W.; Geim, A. K.; Novoselov, K. S. Graphene-Based Liquid Crystal Device. *Nano Lett.* **2008,** 8, 1704-1708.

5.   Hernandez, Y.; Nicolosi, V.; Lotya, M.; Blighe, F. M.; Sun, Z.; De, S.; McGovern, I. T.; Holland, B.; Byrne, M.; Gun'Ko, Y. K.; Boland, J. J.; Niraj, P.; Duesberg, G.; Krishnamurthy, S.; Goodhue, R.; Hutchison, J.; Scardaci, V.; Ferrari, A. C.; Coleman, J. N. High-Yield Production of Graphene by Liquid-Phase Exfoliation of Graphite. *Nat. Nanotechnol.* **2008,** 3, 563-568.

6.   Ciesielski, A.; Samorì, P. Graphene *via* Sonication Assisted Liquid-Phase Exfoliation. *Chem. Soc. Rev.* **2014,** 43, 381-398.

7.   May, P.; Khan, U.; O'Neill, A.; Coleman, J. N. Approaching the Theoretical Limit for Reinforcing Polymers with Graphene. *J. Mater. Chem.* **2012,** 22, 1278-1282.

ACS Nano

8.   Li, X.; Zhang, G.; Bai, X.; Sun, X.; Wang, X.; Wang, E.; Dai, H. Highly Conducting Graphene Sheets and Langmuir–Blodgett Films. *Nat. Nanotechnol.* **2008,** 3, 538-542.

9.   Li, D.; Müller, M. B.; Gilje, S.; Kaner, R. B.; Wallace, G. G. Processable Aqueous Dispersions of Graphene Nanosheets. *Nat. Nanotechnol.* **2008,** 3, 101-105.

10.   Parvez, K.; Yang, S.; Feng, X.; Müllen, K. Exfoliation of Graphene *via* Wet Chemical Routes. *Synth. Met.* **2015,** 210, 123-132.

11.   Kang, J.; Sangwan, V. K.; Wood, J. D.; Hersam, M. C. Solution-Based Processing of Monodisperse Two-Dimensional Nanomaterials. *Acc. Chem. Res.* **2017,** 50, 943-951.

12.   Paton, K. R.; Varrla, E.; Backes, C.; Smith, R. J.; Khan, U.; O'Neill, A.; Boland, C.; Lotya, M.; Istrate, O. M.; King, P.; Higgins, T.; Barwich, S.; May, P.; Puczkarski, P.; Ahmed, I.; Moebius, M.; Pettersson, H.; Long, E.; Coelho, J.; O'Brien, S. E. *et al.* Scalable Production of Large Quantities of Defect-Free Few-Layer Graphene by Shear Exfoliation in Liquids. *Nature Materials* **2014,** 13, 624-630.

13.   Yi, M.; Shen, Z. A Review on Mechanical Exfoliation for the Scalable Production of Graphene. *J. Mater. Chem. A* **2015,** 3, 11700-11715.

14.   Karagiannidis, P. G.; Hodge, S. A.; Lombardi, L.; Tomarchio, F.; Decorde, N.; Milana, S.; Goykhman, I.; Su, Y.; Mesite, S. V.; Johnstone, D. N.; Leary, R. K.; Midgley, P. A.; Pugno, N. M.; Torrisi, F.; Ferrari, A. C. Microfluidization of Graphite and Formulation of Graphene-Based Conductive Inks. *ACS Nano* **2017,** 11, 2742-2755.

15.   Niu, L.; Coleman, J. N.; Zhang, H.; Shin, H.; Chhowalla, M.; Zheng, Z. Production of Two-Dimensional Nanomaterials *via* Liquid-Based Direct Exfoliation. *Small* **2016,** 12, 272-293.

16.   Khan, U.; O'Neill, A.; Lotya, M.; De, S.; Coleman, J. N. High-Concentration Solvent Exfoliation of Graphene. *Small* **2010,** 6, 864-871.

17.   Lotya, M.; King, P. J.; Khan, U.; De, S.; Coleman, J. N. High-Concentration, Surfactant-Stabilized Graphene Dispersions. *ACS Nano* **2010,** 4, 3155-3162.

18.   Shen, J.; He, Y.; Wu, J.; Gao, C.; Keyshar, K.; Zhang, X.; Yang, Y.; Ye, M.; Vajtai, R.; Lou, J.; Ajayan, P. M. Liquid Phase Exfoliation of Two-Dimensional Materials by Directly Probing and Matching Surface Tension Components. *Nano Lett.* **2015,** 15, 5449-5454.

19.   Backes, C.; Higgins, T. M.; Kelly, A.; Boland, C.; Harvey, A.; Hanlon, D.; Coleman, J. N. Guidelines for Exfoliation, Characterization and Processing of Layered Materials Produced by Liquid Exfoliation. *Chem. Mater.* **2017,** 29, 243-255.

20.   Khan, U.; Porwal, H.; O'Neill, A.; Nawaz, K.; May, P.; Coleman, J. N. Solvent-Exfoliated Graphene at Extremely High Concentration. *Langmuir* **2011,** 27, 9077-9082.

21.   Backes, C.; Campi, D.; Szydlowska, B. M.; Synnatschke, K.; Ojala, E.; Rashvand, F.; Harvey, A.; Griffin, A.; Sofer, Z.; Marzari, N.; Coleman, J. N.; O'Regan, D. D. Equipartition of Energy Defines the Size–Thickness Relationship in Liquid-Exfoliated Nanosheets. *ACS Nano* **2019,** 13, 7050-7061.

22.   Ji, L.-J.; Qin, Y.; Gui, D.; Li, W.; Li, Y.; Li, X.; Lu, P. Quantifying the Exfoliation Ease Level of 2D Materials *via* Mechanical Anisotropy. *Chem. Mater.* **2018,** 30, 8732-8738.

23.   Kouroupis-Agalou, K.; Liscio, A.; Treossi, E.; Ortolani, L.; Morandi, V.; Pugno, N. M.; Palermo, V. Fragmentation and Exfoliation of 2-Dimensional Materials: A Statistical Approach. *Nanoscale* **2014,** 6, 5926-5933.

24. Hernandez, Y.; Lotya, M.; Rickard, D.; Bergin, S. D.; Coleman, J. N. Measurement of Multicomponent Solubility Parameters for Graphene Facilitates Solvent Discovery. *Langmuir* **2010,** 26, 3208-3213.

25. Turner, P.; Hodnett, M.; Dorey, R.; Carey, J. D. Controlled Sonication as a Route to *In-Situ* Graphene Flake Size Control. *Sci. Rep.* **2019,** 9, 8710.

26. Xia, Z. Y.; Pezzini, S.; Treossi, E.; Giambastiani, G.; Corticelli, F.; Morandi, V.; Zanelli, A.; Bellani, V.; Palermo, V. The Exfoliation of Graphene in Liquids by Electrochemical, Chemical, and Sonication-Assisted Techniques: A Nanoscale Study. *Adv. Func. Mater.* **2013,** 23, 4684-4693.

27. Liscio, A.; Kouroupis-Agalou, K.; Betriu, X. D.; Kovtun, A.; Treossi, E.; Pugno, N. M.; De Luca, G.; Giorgini, L.; Palermo, V. Evolution of the Size and Shape of 2D Nanosheets during Ultrasonic Fragmentation. *2D Mater.* **2017,** 4, 025017.

28. Halbig, C. E.; Nacken, T. J.; Walter, J.; Damm, C.; Eigler, S.; Peukert, W. Quantitative Investigation of the Fragmentation Process and Defect Density Evolution of Oxo-Functionalized Graphene Due to Ultrasonication and Milling. *Carbon* **2016,** 96, 897-903.

29. Alaferdov, A. V.; Gholamipour-Shirazi, A.; Canesqui, M. A.; Danilov, Y. A.; Moshkalev, S. A. Size-Controlled Synthesis of Graphite Nanoflakes and Multi-Layer Graphene by Liquid Phase Exfoliation of Natural Graphite. *Carbon* **2014,** 69, 525-535.

30. Łoś, S.; Duclaux, L.; Alvarez, L.; Hawełek, Ł.; Duber, S.; Kempiński, W. Cleavage and Size Reduction of Graphite Crystal Using Ultrasound Radiation. *Carbon* **2013,** 55, 53-61.

31.   Salussolia, G.; Barbieri, E.; Pugno, N. M.; Botto, L. Micromechanics of Liquid-Phase Exfoliation of a Layered 2D Material: A Hydrodynamic Peeling Model. *J. Mech. Phys. Solids* **2020,** 134, 103764.

32.   Bracamonte, M. V.; Lacconi, G. I.; Urreta, S. E.; Foa Torres, L. E. F. On the Nature of Defects in Liquid-Phase Exfoliated Graphene. *J. Phys. Chem. C* **2014,** 118, 15455-15459.

33.   Ma, H.; Shen, Z.; Ben, S. Understanding the Exfoliation and Dispersion of MoS_2 Nanosheets in Pure Water. *J. Colloid Interface Sci.* **2018,** 517, 204-212.

34.   Skaltsas, T.; Ke, X.; Bittencourt, C.; Tagmatarchis, N. Ultrasonication Induces Oxygenated Species and Defects onto Exfoliated Graphene. *J. Phys. Chem. C* **2013,** 117, 23272-23278.

35.   Lin, Y.; Williams, T. V.; Xu, T.-B.; Cao, W.; Elsayed-Ali, H. E.; Connell, J. W. Aqueous Dispersions of Few-Layered and Monolayered Hexagonal Boron Nitride Nanosheets from Sonication-Assisted Hydrolysis: Critical Role of Water. *J. Phys. Chem. C* **2011,** 115, 2679-2685.

36.   Gupta, A.; Arunachalam, V.; Vasudevan, S. Liquid-Phase Exfoliation of MoS_2 Nanosheets: The Critical Role of Trace Water. *J. Phys. Chem. Lett.* **2016,** 7, 4884-4890.

37.   Jawaid, A.; Nepal, D.; Park, K.; Jespersen, M.; Qualley, A.; Mirau, P.; Drummy, L. F.; Vaia, R. A. Mechanism for Liquid Phase Exfoliation of MoS_2. *Chem. Mater.* **2016,** 28, 337-348.

38.   Backes, C.; Szydłowska, B. M.; Harvey, A.; Yuan, S.; Vega-Mayoral, V.; Davies, B. R.; Zhao, P.-l.; Hanlon, D.; Santos, E. J. G.; Katsnelson, M. I.; Blau, W. J.; Gadermaier, C.; Coleman, J. N. Production of Highly Monolayer Enriched Dispersions of Liquid-Exfoliated Nanosheets by Liquid Cascade Centrifugation. *ACS Nano* **2016,** 10, 1589-1601.

39.   Papageorgiou, D. G.; Li, Z.; Liu, M.; Kinloch, I. A.; Young, R. J. Mechanisms of Mechanical Reinforcement by Graphene and Carbon Nanotubes in Polymer Nanocomposites. *Nanoscale* **2020,** 12, 2228-2267.

40.   Fugallo, G.; Cepellotti, A.; Paulatto, L.; Lazzeri, M.; Marzari, N.; Mauri, F. Thermal Conductivity of Graphene and Graphite: Collective Excitations and Mean Free Paths. *Nano Lett.* **2014,** 14, 6109-6114.

41.   He, P.; Derby, B. Inkjet Printing Ultra-Large Graphene Oxide Flakes. *2D Mater.* **2017,** 4, 021021.

42.   Rooney, A. P.; Li, Z.; Zhao, W.; Gholinia, A.; Kozikov, A.; Auton, G.; Ding, F.; Gorbachev, R. V.; Young, R. J.; Haigh, S. J. Anomalous Twin Boundaries in Two Dimensional Materials. *Nat. Commun.* **2018,** 9, 3597.

43.   Blind Thrust Fault: Earthquake Hazards Program of the U.S. Geological Survey (Usgs). https://earthquake.usgs.gov/learn/glossary/?term=blind%20thrust%20fault   (accessed 29/10/2019).

44.   Hess, P. Surface Acoustic Waves in Materials Science. *Phys. Today* **2002,** 55, 42-47.

45.   Soule, D. E.; Nezbeda, C. W. Direct Basal‐Plane Shear in Single-Crystal Graphite. *J. Appl. Phys.* **1968,** 39, 5122-5139.

46.   Zhou, G.; Rajak, P.; Susarla, S.; Ajayan, P. M.; Kalia, R. K.; Nakano, A.; Vashishta, P. Molecular Simulation of MoS_2 Exfoliation. *Sci. Rep.* **2018,** 8, 16761.

47.   Motlag, M.; Hu, Y.; Tong, L.; Huang, X.; Ye, L.; Cheng, G. J. Laser-Shock-Induced Nanoscale Kink-Bands in WSe$_2$ 2D Crystals. *ACS Nano* **2019,** 13, 10587-10595.

48.   Meng, L.; Li, Y.; Liu, T. S.; Zhu, C.; Li, Q. Y.; Chen, X.; Zhang, S.; Zhang, X.; Bao, L.; Huang, Y.; Xu, F.; Ruoff, R. S. Wrinkle Networks in Exfoliated Multilayer Graphene and Other Layered Materials. *Carbon* **2020,** 156, 24-30.

49.   Suslick, K. S. Sonochemistry. *Science* **1990,** 247, 1439.

50.   Ciesielski, A.; Haar, S.; Aliprandi, A.; El Garah, M.; Tregnago, G.; Cotella, G. F.; El Gemayel, M.; Richard, F.; Sun, H.; Cacialli, F.; Bonaccorso, F.; Samorì, P. Modifying the Size of Ultrasound-Induced Liquid-Phase Exfoliated Graphene: From Nanosheets to Nanodots. *ACS Nano* **2016,** 10, 10768-10777.

51.   Ma, L.; Wang, J.; Ding, F. Strain-Induced Orientation-Selective Cutting of Graphene into Graphene Nanoribbons on Oxidation. *Angew. Chem. Int. Ed.* **2012,** 51, 1161-1164.

52.   Kosynkin, D. V.; Higginbotham, A. L.; Sinitskii, A.; Lomeda, J. R.; Dimiev, A.; Price, B. K.; Tour, J. M. Longitudinal Unzipping of Carbon Nanotubes to Form Graphene Nanoribbons. *Nature* **2009,** 458, 872-6.

53.   Xie, L.; Wang, H.; Jin, C.; Wang, X.; Jiao, L.; Suenaga, K.; Dai, H. Graphene Nanoribbons from Unzipped Carbon Nanotubes: Atomic Structures, Raman Spectroscopy, and Electrical Properties. *J. Am. Chem. Soc.* **2011,** 133, 10394-7.

54.   Koskinen, P.; Malola, S.; Häkkinen, H. Self-Passivating Edge Reconstructions of Graphene. *Phys. Rev. Lett.* **2008,** 101, 115502.
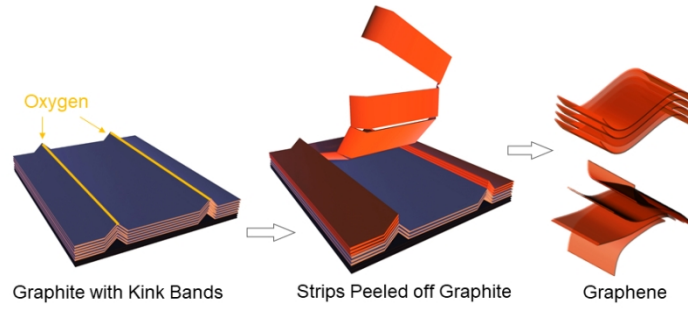
55. van Engers, C. D.; Cousens, N. E. A.; Babenko, V.; Britton, J.; Zappone, B.; Grobert, N.; Perkin, S. Direct Measurement of the Surface Energy of Graphene. *Nano Lett.* **2017,** 17, 3815-3821.

56. Abrahamson, J. The Surface Energies of Graphite. *Carbon* **1973,** 11, 337-362.

57. Wang, W.; Dai, S.; Li, X.; Yang, J.; Srolovitz, D. J.; Zheng, Q. Measurement of the Cleavage Energy of Graphite. *Nat. Commun.* **2015,** 6, 7853.

58. Annett, J.; Cross, G. L. Self-Assembly of Graphene Ribbons by Spontaneous Self-Tearing and Peeling from a Substrate. *Nature* **2016,** 535, 271-5.

59. Niu, L.; Li, M.; Tao, X.; Xie, Z.; Zhou, X.; Raju, A. P. A.; Young, R. J.; Zheng, Z. Salt-Assisted Direct Exfoliation of Graphite into High-Quality, Large-Size, Few-Layer Graphene Sheets. *Nanoscale* **2013,** 5, 7202-7208.

60. Lotya, M.; Hernandez, Y.; King, P. J.; Smith, R. J.; Nicolosi, V.; Karlsson, L. S.; Blighe, F. M.; De, S.; Wang, Z.; McGovern, I. T.; Duesberg, G. S.; Coleman, J. N. Liquid Phase Production of Graphene by Exfoliation of Graphite in Surfactant/Water Solutions. *J. Am. Chem. Soc.* **2009,** 131, 3611–3620.

61. Ueberricke, L.; Coleman, J. N.; Backes, C. Robustness of Size Selection and Spectroscopic Size, Thickness and Monolayer Metrics of Liquid-Exfoliated WS_2. *Phys. Status Solidi B* **2017,** 254, 1700443.

62. Kresse, G.; Furthmuller, J. Efficiency of *Ab-Initio* Total Energy Calculations for Metals and Semiconductors Using a Plane-Wave Basis Set. *Comp. Mater. Sci.* **1996,** 6, 15-50.

63.   Perdew, J. P.; Burke, K.; Ernzerhof, M. Generalized Gradient Approximation Made Simple. *Phys. Rev. Lett.* **1996,** 77, 3865-3868.

64.   Blochl, P. E. Projector Augmented-Wave Method. *Phys. Rev. B* **1994,** 50, 17953-17979.

65.   Tkatchenko, A.; Scheffler, M. Accurate Molecular van der Waals Interactions from Ground-State Electron Density and Free-Atom Reference Data. *Phys. Rev. Lett.* **2009,** 102, 073005.

1
2
3
4
5
6
7
8
9
10
11
12
13
14
15
16
17
18
19
20
21
22
23
24
25
26
27
28
29
30
31
32
33
34
35
36
37
38
39
40
41
42
43
44
45
46
47
48
49
50
51
52
53
54
55
56
57
58
59
60

338x190mm (96 x 96 DPI)